J BONE ONCOL 48 (2024) 100626

Contents lists available at ScienceDirect

Journal of Bone Oncology

journal homepage: www.elsevier.com/locate/jbo

An enhanced AlexNet-Based model for femoral bone tumor classification and diagnosis using magnetic resonance imaging

Xu Chen [a,1], Hongkun Chen [a,1], Junming Wan [a], Jianjun Li [b,*], Fuxin Wei [a,*]

[a] Department of Orthopedic Surgery, The Seventh Affiliated Hospital, Sun Yat-sen University, Shenzhen, Guangdong 518107, PR China
[b] Department of Orthopedic Surgery, Shengjing Hospital of China Medical University, Shenyang, Liaoning 110004, PR China

HIGHLIGHTS

- **Optimized AlexNet Model for Femoral Bone Tumor Classification:** The article introduces an optimized deep learning model based on AlexNet for the accurate classification of femoral bone tumors. This model aims to address the challenges associated with the infrequent occurrence and diverse imaging characteristics of bone tumors.
- **Architectural Enhancements and Batch Normalization:** The proposed model includes architectural modifications, such as the incorporation of Batch Normalization (BN) after specific convolutional filters. Batch Normalization is introduced to address issues related to data shifts caused by ReLU functions, promoting network convergence and improving overall performance.
- **Performance Evaluation Metrics:** The study conducts comparative experiments with various existing methods and evaluates the algorithm's performance using metrics such as accuracy, precision, sensitivity, specificity, F-measure, ROC curves, and AUC values. The analysis demonstrates the algorithm's advantages, including low feature dimension, robust generalization, and exceptional overall detection capabilities.
- **Outstanding Performance in Tumor Staging:** The results highlight the exceptional performance of the introduced algorithm in tumor staging, with an accuracy of 98.34%, sensitivity of 97.26%, specificity of 95.74%, and an F1 score of 96.37. The algorithm's ability to classify femoral bone tumors surpasses several existing methods, emphasizing its clinical relevance.
- **Significant Contribution to Medical Image Classification:** The article concludes by emphasizing the significance of the research in the field of medical image classification. The optimized AlexNet model offers an efficient automated classification solution, contributing to the advancement of artificial intelligence in bone tumor classification. The study provides a valuable tool for medical professionals, potentially improving patient care and treatment outcomes in orthopedics.

ARTICLE INFO

Keywords:
AlexNet
Femoral bone tumors
Convolutional neural networks
Medical image classification
Diagnosis

ABSTRACT

Objective: Bone tumors, known for their infrequent occurrence and diverse imaging characteristics, require precise differentiation into benign and malignant categories. Existing diagnostic approaches heavily depend on the laborious and variable manual delineation of tumor regions. Deep learning methods, particularly convolutional neural networks (CNNs), have emerged as a promising solution to tackle these issues. This paper introduces an enhanced deep-learning model based on AlexNet to classify femoral bone tumors accurately.
Methods: This study involved 500 femoral tumor patients from July 2020 to January 2023, with 500 imaging cases (335 benign and 165 malignant). A CNN was employed for automated classification. The model framework encompassed training and testing stages, with 8 layers (5 Conv and 3 FC) and ReLU activation. Essential architectural modifications included Batch Normalization (BN) after the first and second convolutional filters. Comparative experiments with various existing methods were conducted to assess algorithm performance in tumor staging. Evaluation metrics encompassed accuracy, precision, sensitivity, specificity, F-measure, ROC curves, and AUC values.
Results: The analysis of precision, sensitivity, specificity, and F1 score from the results demonstrates that the method introduced in this paper offers several advantages, including a low feature dimension and robust generalization (with an accuracy of 98.34 %, sensitivity of 97.26 %, specificity of 95.74 %, and an F1 score of 96.37). These findings underscore its exceptional overall detection capabilities. Notably, when comparing

* Corresponding authors at: Department of Orthopedic Surgery, Shengjing Hospital of China Medical University, Shenyang, Liaoning 110004, PR China. Department of Orthopedic Surgery, The Seventh Affiliated Hospital, Sun Yat-sen University, Shenzhen, Guangdong 518107, PR China.
E-mail addresses: lij2046@126.com (J. Li), weifuxin@sysush.com (F. Wei).
[1] These authors contributed equally to this work.

https://doi.org/10.1016/j.jbo.2024.100626
Received 24 April 2024; Received in revised form 22 July 2024; Accepted 25 July 2024
Available online 3 August 2024

various algorithms, they generally exhibit similar classification performance. However, the algorithm presented in this paper stands out with a higher AUC value (AUC=0.848), signifying enhanced sensitivity and more robust specificity.

Conclusion: This study presents an optimized AlexNet model for classifying femoral bone tumor images based on convolutional neural networks. This algorithm demonstrates higher accuracy, precision, sensitivity, specificity, and F1-score than other methods. Furthermore, the AUC value further confirms the outstanding performance of this algorithm in terms of sensitivity and specificity. This research makes a significant contribution to the field of medical image classification, offering an efficient automated classification solution, and holds the potential to advance the application of artificial intelligence in bone tumor classification.

1. Introduction

Bone tumors are a relatively low-incidence type of disease within the field of oncology, typically presenting with a variety of morphological imaging features and a high degree of heterogeneity. The primary treatment approaches for bone tumors include neoadjuvant radiotherapy, chemotherapy, and surgical interventions [1]. Accurately segmenting tumor lesion regions from bone tumor CT and MRI images [2] is of paramount importance for preoperative planning of neoadjuvant chemoradiotherapy and postoperative treatment evaluation. However, manual delineation of tumor regions is time-consuming and labor-intensive. Additionally, the results of tumor delineation can be influenced by various factors, such as the subjective experience and working conditions of different radiologists, and the delineation results may lack reproducibility [3]. Therefore, there is an urgent clinical need to achieve automatic segmentation of tumor regions and make sound interpretations. Currently, CNNs are widely applied for deep learning of tumor classification in this regard [4].

The application of AI in bone tumor classification dates back to an earlier period. As early as 1980, Lodwick et al. [5] used computer models to determine bone tumor classification. In 1994, Reinus et al. [6] researched using neural network models to diagnose bone tumors, encoding the imaging features of 709 lesions into a predefined database. The accuracy of this model in distinguishing between benign and malignant lesions reached 85 %. In 2017, Do et al. [7] developed a Bayesian model to predict bone tumor diagnosis and differential diagnosis on 710 X-ray images, achieving a high accuracy of 62 % for correct diagnosis and 80 % for differential diagnosis.

Note that AI is extensively applied to delineate bone tumor boundaries. Huang et al. [8] introduced an automatic tumor boundary segmentation method based on a multiple supervised fully convolutional network (MSFCN) model. When compared to manually segmented results in 405 cases of bone tumors, it achieved an average Dice similarity coefficient (DSC) of 87.80 %, average sensitivity of 86.88 %, average Hammoude measure (HM) of 19.81 %, and an F1 score of 0.908. This outperforms the fully convolutional network (FCN) model, U-Net, and holistically-nested edge detection (HED) method regarding DSC, sensitivity, HM, and F1 score. This algorithm assists in quickly and accurately delineating tumor boundaries, aiding physicians in devising more precise treatment plans. The team [9] also proposed a bone tumor image segmentation method based on a multiple-supervised residual network (MSRN) model. Compared to the best segmentation results from advanced algorithms like FCN and U-Net, MSRN improved the DSC coefficient by 8.78 %, sensitivity by 7.83 %, and F1 score by 6.71 %.

The application of AI in predicting postoperative recurrence in bone tumors started relatively late. He et al. [10] utilized CNN models to predict postoperative local recurrence in 56 patients with confirmed pathology of giant cell tumors of bone based on MRI images and clinical data. They also incorporated patient characteristics (age, tumor location, etc.) to establish a binary logistic regression model for predicting tumor recurrence. Comparing the CNN, CNN regression model, and radiologist diagnoses, the accuracy rates for CNN and CNN regression models were 75.5 % and 78.6 %, respectively, surpassing radiologists' 64.3 %. Sensitivity for CNN and CNN regression models was 85.7 % and 87.5 %, higher than radiologists' 58.3 %. This research suggests that CNNs hold predictive value for postoperative giant cell tumor recurrence, and the binary regression model incorporating patient characteristics enhances the accuracy of predicting tumor recurrence.

In practice, AI has found numerous applications in bone tumor image recognition and segmentation, offering efficiency in image processing [11]. However, there is room for improvement in its accuracy, particularly for identifying smaller bone tumor regions, which may require substantial data for model optimization [12].

Dealing with the demanding task of diagnosing femoral bone tumors from various medical images presents a significant challenge for medical professionals. Maintaining consistent levels of accuracy and efficiency can be a formidable endeavor, potentially leading to diagnostic errors. The regions affected by femoral bone tumors, such as osteosarcomas and osteochondromas, exhibit striking similarities in appearance and texture during the early stages of tumor development. Hence, computer-aided diagnostic technology is crucial for accurately classifying femoral bone tumors.

Computer-aided diagnosis technology predominantly relies on machine learning and deep learning methodologies when dealing with femoral bone tumors. Machine learning methods require the manual design of features, fraught with complexities and low recognition accuracy. With the continuous advancements in deep learning, CNNs can autonomously acquire high-level features, which have consistently demonstrated superior performance compared to manually designed low-level features in numerous studies[13]. VGG, AlexNet, and ResNet have broad applications among the convolutional neural network techniques. However, VGG and the model structure of AlexNet are noted for their simplicity and less-than-optimal outcomes.

2. Material and methods

Using a CNN to perform the automated classification task of femoral bone pathological images. The overall model framework is illustrated in Fig. 1 and can be divided into the training and testing stages. The neural network is trained on an augmented training dataset and, ultimately, its recognition performance is evaluated on the testing dataset.

2.1. Data augmentation

The most effective way to improve model generalization is by training it on a large-scale dataset. However, the process of creating medical pathological images is labor-intensive, expensive to annotate, and challenging to obtain. In deep learning, data augmentation methods are typically used to address the issue of limited data [14].

Geometric transformations are employed for data augmentation in this context. Utilizing the built-in data augmentation functions are subjected to translation, scaling, rotation, horizontal flipping, and vertical flipping. This helps expand the dataset in each batch, mitigating the impact of data scarcity. Fig. 2 illustrates the results of data augmentation.

2.2. AlexNet network architecture

AlexNet (Fig. 2) is a convolutional neural network model widely used for image classification. The network architecture of AlexNet is illustrated in Fig. 3. The network comprises 8 layers, including 5 convolutional layers (labeled Conv) and 3 fully connected layers (labeled FC). ReLU is used as the activation function to enhance the network's nonlinearity. The network also includes three pooling layers (labeled as MaxPool), located after the first, second, and fifth convolutional layers, with the output size of the pooling layers being half of their input size. The third and fourth convolutional layers maintain the same input and output sizes. The features output from the final convolutional layer are flattened and passed into the fully connected layers, with each of the first two fully connected layers consisting of 4096 neurons. The SoftMax function is applied to the output of the last fully connected layer to generate a feature vector, representing the final prediction results as a probability vector.

Due to the use of the ReLU function as the activation function in the network. The output is entirely zero when the input feature values are less than zero. This can introduce some bias to the data, causing a shift in the original data distribution, thereby increasing the network's training time and potentially reducing its recognition accuracy.

2.3. Batch normalization

Training deep neural networks is highly intricate, where even minor adjustments in the early layers can have a cascading effect on subsequent layers. Fundamentally, neural network learning revolves around understanding data distributions. When input data distribution to a network layer undergoes alterations, that layer must dynamically adapt to learn the new data distribution. A training data distribution that undergoes constant fluctuations during the training process can significantly impact the efficiency of network training. The BN algorithm, proposed in reference [15], is designed to reduce data shifts caused by ReLU functions, addressing the issue of changing data distributions during training. This, in turn, accelerates network convergence and improves network performance. BN achieves feature normalization by computing the mean and variance within a small batch of data. The detailed process of the BN algorithm is outlined in Table 1.

Input: All samples in a mini-batch:

$$B = \{x_1, \cdots, x_m\} \tag{1}$$

Output: Normalized sample values:

$$y_i = \{BN_{\gamma,\beta}\} \tag{2}$$

Mean of the samples in the mini-batch:

$$\mu_B = \frac{1}{m}\sum_{i=1}^{m} x_i \tag{3}$$

Variance of the samples in the mini-batch:

$$\sigma^2{}_B = \frac{1}{m}\sum_{i=1}^{m}(x_i - \mu_B)^2 \tag{4}$$

Normalization process:

$$\widehat{x}_i = \frac{x_i - \mu_B}{\sqrt{\sigma^2{}_B + \varepsilon}} \tag{5}$$

Incorporating scaling and offset:

$$y_i = \gamma\widehat{x}_i + \beta = BN_{\gamma,\beta}(x_i) \tag{6}$$

In the provided equation, β represents a small batch sample set, μ_B represents the mean of this sample set, σ^2 denotes the variance, and ε is a constant used to enhance numerical stability. The expectation and variance are relative to the training set in practical applications. The variable x_i represents the standardized feature values, but at this point, the content represented by these feature values has been altered. To address this issue, it is necessary to transform and reconstruct z to introduce two learnable parameters, γ and β. The output feature y_i is obtained by scaling and shifting the x_i, thereby restoring the original feature distribution that the network needs to learn. The values of γ and β are updated as the network weights are updated, and they can be calculated using the following equations.

$$r^{i} = \sqrt{Var[x(k)]} \tag{7}$$

$$\beta^{i} = E[x(i)] \tag{8}$$

The convolutional layers extract features that can be both positive and negative. However, the ReLU function discards negative features, which introduces a level of bias. This bias tends to increase as the network deepens, potentially impacting the network's decision-making accuracy. To mitigate this, it is recommended to position the BN layer

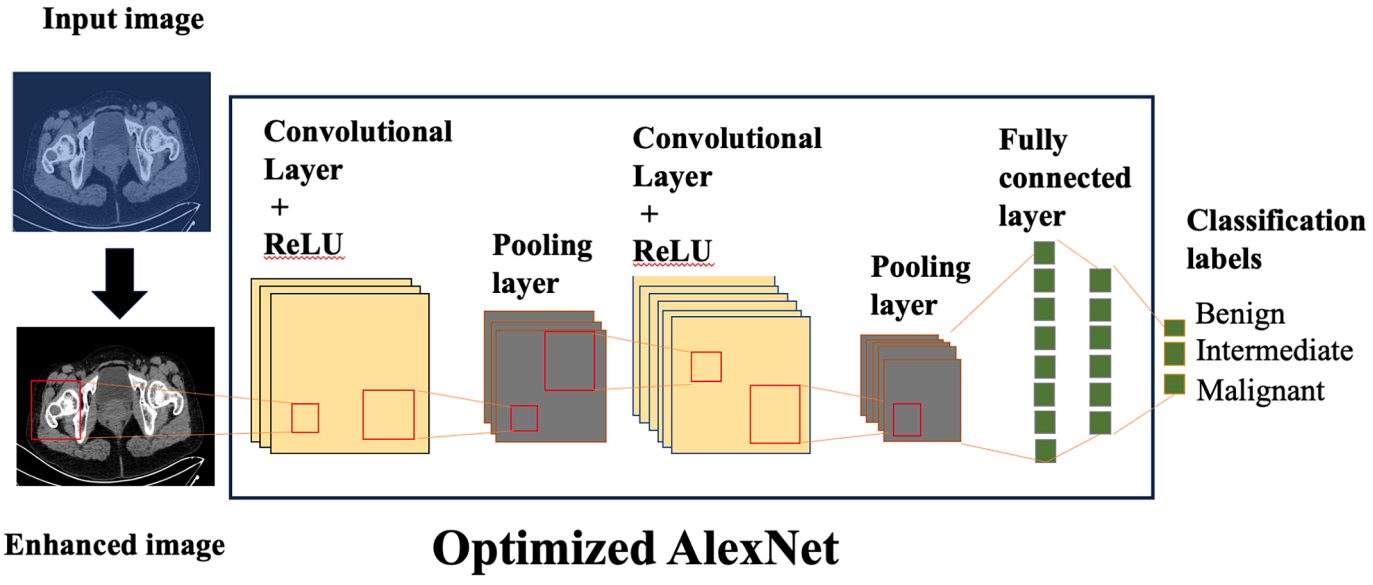

Fig. 1. depicts the femoral bone pathological image classification workflow using the optimized AlexNet.

between the convolutional layer and the activation function. The BN algorithm normalizes features before activation, reducing the introduced bias, accelerating network convergence, and improving the network's generalization ability.

2.4. Optimized AlexNet network

In this experiment, we introduced several enhancements to the foundational architecture of the AlexNet network, as depicted in Fig. 3. Fig. 4 illustrates the structural unit of the convolutional layer with the integration of BN. Before entering the activation unit, feature vectors resulting from the first and second convolutional filters undergo normalization using the BN algorithm. This structural unit effectively replaces the original convolutional layer structure in the AlexNet network. Choosing an optimal batch size tailored to the specific dataset characteristics significantly improves recognition accuracy. For this experiment, a batch size of 32 was carefully selected.

2.5. Network parameter settings

For the AlexNet network, ensuring that the input image size is essential. In this experiment, the femoral bone pathological images, initially sized at 460x700 pixels, were resized to 224x224 pixels. The convolutional layers were initialized using a normal distribution during the training process. L2 regularization was applied to the last three convolutional layers with a penalty factor of 0.0001 for input features. Stochastic Gradient Descent (SGD) was selected as the optimizer for the network, with a learning rate set to 0.01. Since the fully connected layers in AlexNet introduce many parameters, which increases the risk of overfitting, Dropout was applied after the first two fully connected layers. During the network's training process, Dropout allows the network to randomly "deactivate" specific neurons with a specified probability. This randomness in neuron deactivation ensures that not every pair of hidden nodes appears together at each weight update. Consequently, the weight updates are no longer dependent on the combined actions of fixed-related hidden nodes, which prevents the situation where some features are only practical under specific conditions. A dropout rate of 60 % was set for this experiment, which led to excellent results.

2.6. GoogLeNet

GoogLeNet is a CNN model with a network depth of 22 layers. This model significantly reduces data computation complexity compared to classic networks like LeNet and AlexNet. In contrast to emerging networks like VGG, it offers faster training speed while maintaining high recognition accuracy. Therefore, the GoogLeNet model is better suited for datasets with more straightforward features, such as the RCP dataset.

InceptionV1 is a fundamental building block of GoogLeNet, and its structure is illustrated within the dashed box in Fig. 2. The core idea of this module is as follows: 1) It aggregates convolutional layers of different scales to gather visual information of various sizes. 2) It reduces the dimensionality of high-dimensional matrices to promote feature extraction at different scales, ultimately achieving multi-scale feature fusion.

GoogLeNet consists of 9 Inception modules, and all convolutional layers incorporate Rectified Linear Units (ReLU) for rectification. Additionally, the structure includes average pooling layers and Dropout layers, serving not only to reduce dimensions but also to prevent overfitting.

3. Empirical analysis

3.1. Experimental dataset

This research involved 500 patients with femoral tumors treated at small, medium, and large hospitals from July 2020 to January 2023. The patients had an age range of 59 to 87 years, with an average age of 63.2 ± 6.8 years. The tumor diameters ranged from 0.7 to 3.9 cm, with an average diameter of 3.2 ± 0.7 cm. Inclusion criteria were as follows: (1)

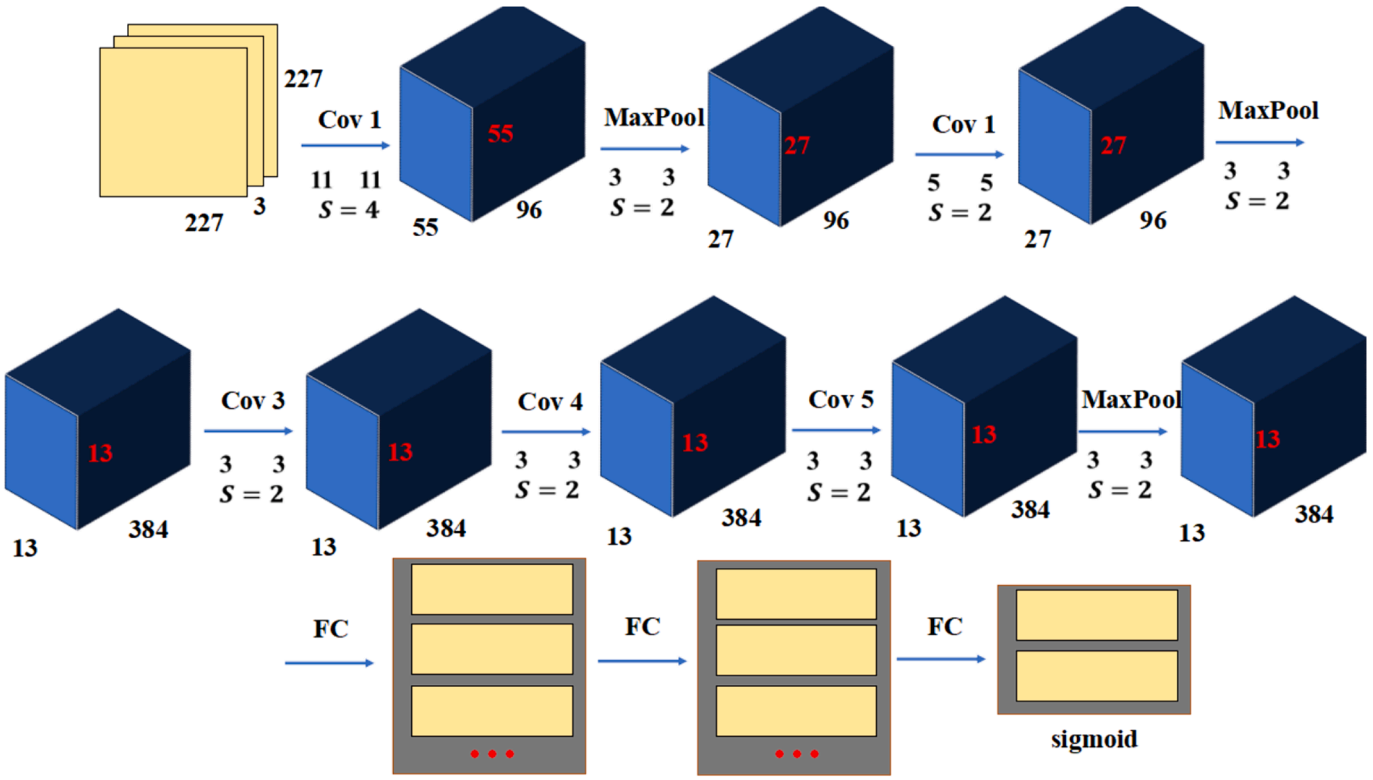

Fig. 2. AlexNet model structure.

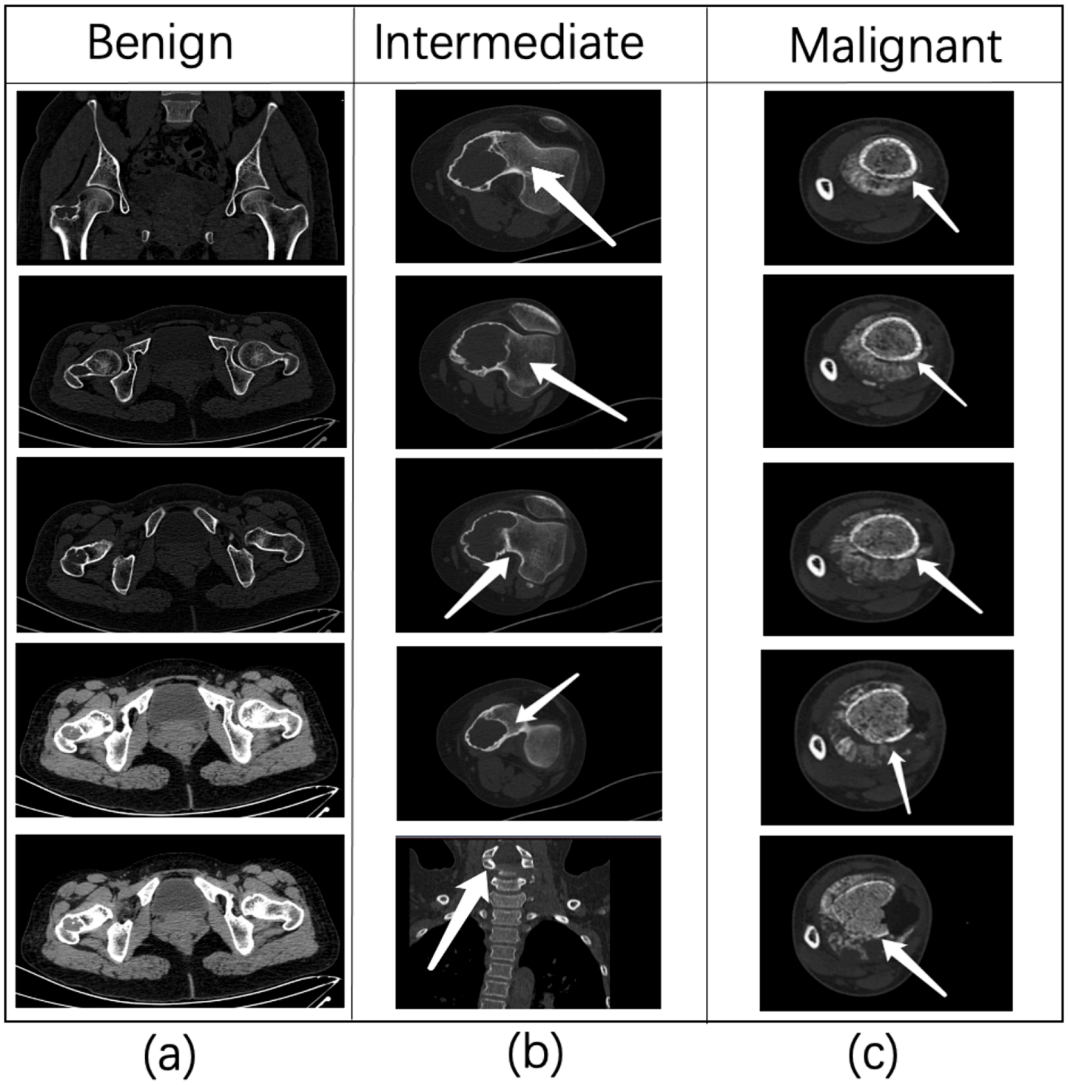

Fig. 3. Partial display of a dataset containing CT images of the tibia and femur. Part a represents a benign bone tumor; part b represents a neutral bone tumor; and part c represents a malignant tumor. The white arrows point to the location of the tumor.

Table 1
Configuration of data environment.

Project	Parameter
Training set	300
Test set	200
Software environment	Python
Hardware configuration	NVIDIA GeForce GTX 1060. Video memory capacity: 3 GB

all patients had single tumor masses, (2) preoperative MRI classification examinations were conducted, (3) clinical data were complete, and (4) all participants provided informed consent for the study and willingly cooperated. Exclusion criteria included (1) concurrent presence of other tumors, (2) blood system diseases, (3) mental illnesses, and (4) withdrawal from the study by participants.

The dataset includes 500 imaging cases, consisting of 335 benign and 165 malignant cases. Specific cases of benign and malignant tumors are illustrated in Fig. 3, where Fig. 3(a) are examples of benign tumors, Fig. 3(b) are examples of intermediate tumors, and Fig. 3(c) are examples of malignant tumors.

3.2. Experimental data preprocessing

Due to the issue of imbalanced benign and malignant image counts in the sample dataset, preprocessing of experimental data is required. The preprocessing steps are as follows: Step 1: Tumor region extraction, extracting the tumor region from the image data, and selecting a rectangular region of 20 pixels. Step 2: Image binarization applies binarization to the image data, retaining the largest connected region. This region performs sequential operations of opening, closing, and hole filling. Step 3: Data augmentation increases the samples by applying rotations and mirroring. For the experimental validation, we utilized the dataset for both training and testing purposes. This was achieved through a 10-fold cross-validation approach comprising 1000 iterations. A comprehensive overview of the specific experimental environment configuration parameters can be found in Table 1.

3.3. Results analysis

To validate the performance of the algorithm proposed in this paper and determine its accuracy in the staging of femoral tumors, comparative experiments were conducted with multiple existing algorithms (Fig. 4). The comprehensive performance of the algorithm was evaluated using various metrics, including accuracy, precision, sensitivity,

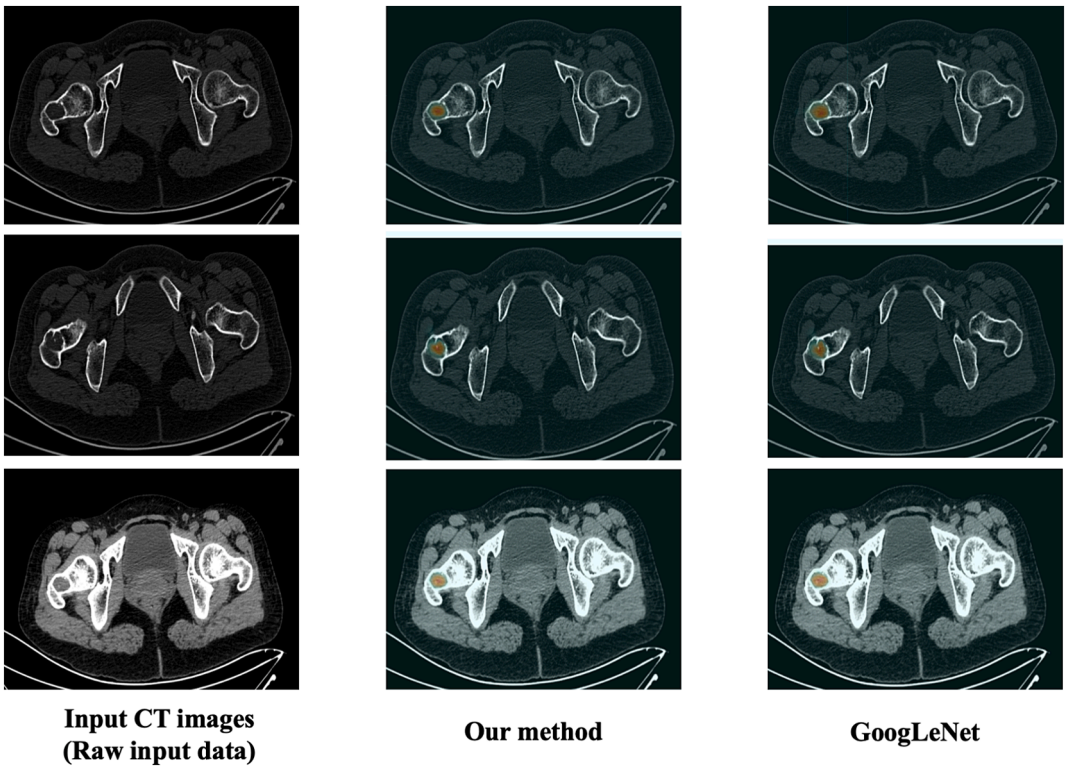

Fig. 4. Comparison of Femoral Tumor Recognition Results Based on Different Algorithms.

specificity, F-measure, ROC curves, and AUC values. Table 3 displays a comparative analysis of accuracy results between the algorithm introduced in this paper and the other comparative algorithms.

As shown in Table 2, it is clear that, among the five methods, the algorithm presented in this paper exhibits the highest accuracy. Additional assessment metrics, including precision, sensitivity, specificity, F1-score, and AUC, will be utilized to provide a more comprehensive evaluation of this algorithm's performance. The detailed evaluation results are provided in the table below.

From the calculated results of precision, sensitivity, specificity, and F1 score, it can be observed that the proposed method in this paper possesses the advantages of low feature dimension and strong generalization (ACC=98.34, SEN=97.26, SPE=95.74, F1 = 96.37), indicating its overall solid detection capability.

In machine learning, the ROC curve and AUC value are commonly used to assess the performance of machine learning algorithms. While the ROC curve provides a qualitative performance representation, the AUC value is typically used to provide a quantitative description of the ROC curve. The AUC values for the algorithm above and the algorithm proposed in this paper are compared in Table 3.

From Table 3, the classification performance of the algorithms is generally comparable. However, the algorithm proposed in this paper exhibits a higher AUC value (AUC=0.848), indicating that it possesses greater sensitivity and more robust specificity.

Table 2
Overall performance comparison of the proposed algorithm with an existing technique.

Performance metrics	Models used for comparison	
	Our method	GoogLeNet
Accuracy	98.34	96.58
Sensitivity	97.26	96.27
Specificity	95.74	92.58
F1 value	96.37	93.69

Table 3
Comparison of AUC of the proposed algorithm with an existing technique.

Performance metrics	Models used for comparison	
	Our method	GoogLeNet
AUC	0.848	0.688

4. Discussion

While the study above presents an optimized AlexNet deep learning model for the precise classification of femoral bone tumors, several limitations still need to be considered. Firstly, the classification of femoral bone tumors remains a complex challenge due to the various morphological and feature variations presented by different tumor types [16]. This complexity level could result in misclassifications or challenges in achieving precise classification. Deep learning models typically demand a significant quantity of annotated data for training to attain high accuracy. However, obtaining a substantial volume of labeled data for rare types of tumors could be a limiting factor.

Furthermore, despite the excellent performance of AlexNet in image classification tasks, concerns arise regarding the model's interpretability and transparency in the context of medical image classification [17]. Medical practitioners and clinical experts often require understanding the model's decision-making process to validate results and make clinical decisions. Therefore, explaining the decision process of deep learning models and providing confidence measures are crucial.

Another possible constraint pertains to the model's generalization performance. Although the studies above demonstrate remarkable results, it is essential to conduct additional validation to ascertain the model's capacity to generalize across various datasets and clinical contexts. Medical images are susceptible to variations stemming from differences in devices and imaging conditions, which could potentially cause the model's performance to be negatively affected [18].

Furthermore, it is essential to highlight that due to the regulatory and ethical complexities within the medical domain, the clinical

implementation of deep learning models demands stringent oversight and validation to guarantee both safety and efficacy [19]. This necessitates close collaboration with healthcare professionals and regulatory bodies.

Although deep learning models such as AlexNet have made significant strides in femoral bone tumor classification, several limitations must be addressed, including data acquisition, interpretability, generalization performance, and regulatory concerns, to make them more feasible and reliable in clinical practice. Future research should focus on tackling these challenges to enhance further the potential of deep learning in tumor classification [20].

In summary, deep learning models hold immense potential in classifying femoral bone tumors, but they still face numerous challenges within the medical field. Future research should address issues related to data acquisition, interpretability, generalization performance, and regulatory compliance to enhance the feasibility and reliability of these models in medical practice [21]. This will contribute to advancements in medical image classification, ultimately providing better healthcare services and treatment options for orthopedic patients [22].

5. Conclusion

The results of this study demonstrate the effectiveness of the optimized AlexNet-based neural network in classifying femoral bone tumors. Notably, it outperforms other comparative algorithms in terms of accuracy. Furthermore, the algorithm exhibits superior precision, sensitivity, specificity, and F1-score. Using the ROC curve and AUC values confirms that the proposed algorithm excels in both sensitivity and specificity.

This research contributes to medical image classification and provides a valuable tool for medical professionals diagnosing femoral bone tumors. Implementing an automated classification system, underpinned by an optimized deep learning model, presents a promising avenue for enhancing the precision and expediency of tumor diagnosis, ultimately leading to improved patient care. Further research may focus on expanding the dataset and exploring additional optimization techniques to continue advancing the capabilities of AI in bone tumor classification.

CRediT authorship contribution statement

Xu Chen: Writing – original draft, Project administration, Methodology, Funding acquisition. **Hongkun Chen:** Writing – review & editing, Writing – original draft, Data curation, Conceptualization. **Junming Wan:** Validation, Supervision, Software, Resources, Methodology, Data curation. **Jianjun Li:** Project administration, Funding acquisition, Formal analysis, Data curation. **Fuxin Wei:** Writing – review & editing, Supervision, Funding acquisition, Formal analysis.

Declaration of competing interest

The authors declare that they have no known competing financial interests or personal relationships that could have appeared to influence the work reported in this paper.

Acknowledgement

Our research was supported by Guangdong Basic and Applied Basic Research Foundation(Grant No.2021A1515110882), Postdoctoral research grants to stay (come to) Shenzhen(Grant No.00201381029), Joint Funds of the Zhejiang Provincial Natural Science Foundation of China(Grant No. LBY21H170001),Shenzhen Key Laboratory of Bone Tissue Repair and Translational Research (NO. ZDSYS20230626091402006), Guangdong Basic and Applied Basic Research Foundation (Grant No. 2021B1515140056).

Author contributions

X.C: Conception and design, financial support, final approval of the manuscript.

F.X Wei: Conception and design, financial support, final approval of the manuscript. H.K Chen: administrative support, collection and assembly of data, data analysis and interpretation and manuscript writing.

J.M Wan: administrative support, collection and assembly of data and revise manuscript.

J.J Li: financial support and final approval of manuscript.

Ethical approval

All human subjects in this study have given their written consent to participate in our research.

References

[1] G. Feeney, R. Sehgal, M. Sheehan, et al., Neoadjuvant radiotherapy for rectal cancer management[J], World Journal of Gastroenterology 25 (33) (2019) 4850.
[2] X. Deng, Y. Zhu, S. Wang, Y. Zhang, H. Han, D. Zheng, Z. Ding, K.K.L. Wong, CT and MRI Determination of Intermuscular Space within Lumbar Paraspinal Muscles at Different Intervertebral Disc Level, PLoS ONE 10 (10) (2015) e0140315.
[3] P. Bos, M.W.M. van den Brekel, M. Taghavi, et al., The largest diameter delineations can substitute 3D tumor volume for radiomics predicting human papillomavirus status on oropharyngeal cancer MRI [J], Physica Medica 101 (2022) 36–43.
[4] Z. Akkus, A. Galimzianova, A. Hoogi, et al., Deep learning for brain MRI segmentation: state of the art and future directions[J], Journal of Digital Imaging 30 (2017) 449–459.
[5] G.S. Lodwick, A.J. Wilson, C. Farrell, et al., Estimating rate of growth in bone lesions: observer performance and error[J], Radiology 134 (3) (1980) 585–590.
[6] W.R. Reinus, A.J. Wilson, B. Kalman, et al., Diagnosis of focal bone lesions using neural networks[J], Invest Radiol 29 (6) (1994) 606–611.
[7] B.H. Do, C. Langlotz, C.F. Beaulieu, Bone tumor diagnosis using a naïve Bayesian model of demographic and radiographic features[J], J Digit Imaging 30 (5) (2017) 640–647.
[8] L. Huang, W. Xia, B. Zhang, et al., MSFCN-multiple supervised fully convolutional networks for the osteosarcoma segmentation of CT images[J], Comput Methods Programs Biomed 143 (2017) 67–74.
[9] R. Zhang, L. Huang, W. Xia, et al., Multiple supervised residual network for osteosarcoma segmentation in CT images[J], Comput Med Imaging Graph 63 (2018) 1–8.
[10] Y. He, J. Guo, X. Ding, et al., Convolutional neural network to predict the local recurrence of giant cell tumor of bone after curettage based on pre-surgery magnetic resonance images[J], Eur Radiol 29 (10) (2019) 5441–5451.
[11] W.L. Bi, A. Hosny, M.B. Schabath, et al., Artificial intelligence in cancer imaging: clinical challenges and applications[J], CA: a Cancer Journal for Clinicians 69 (2) (2019) 127–157.
[12] G.D. Rubin, Data explosion: the challenge of multidetector-row CT[J], European Journal of Radiology 36 (2) (2000) 74–80.
[13] T. Kattenborn, J. Leitloff, F. Schiefer, et al., Review on Convolutional Neural Networks (CNN) in vegetation remote sensing[J], ISPRS Journal of Photogrammetry and Remote Sensing 173 (2021) 24–49.
[14] Z. Tang, M. Sui, X. Wang, et al., Theory-guided Deep Neural Network for boiler 3-D NOx concentration distribution prediction[J], Energy 2024 (2024) 131500.
[15] S. Ioffe, C. Szegedy, Batch normalization: Accelerating deep network training by reducing internal covariate shift[C]//International conference on machine learning, Pm (2015) 448–456.
[16] K.G. Thompson, R.R. Pool, Tumors of bones[J], Tumors in Domestic Animals 4 (2002) 245–317.
[17] A. Singh, S. Sengupta, V. Lakshminarayanan, Explainable deep learning models in medical image analysis[J], Journal of Imaging 6 (6) (2020) 52.
[18] J. De Fauw, J.R. Ledsam, B. Romera-Paredes, et al., Clinically applicable deep learning for diagnosis and referral in retinal disease[J], Nature Medicine 24 (9) (2018) 1342–1350.
[19] McCracken M D, Anderson J A, A. Stephenson E, et al. A research ethics framework for the clinical translation of healthcare machine learning[J]. The American Journal of Bioethics, 2022, 22(5): 8-22.
[20] P. Papadimitroulas, L. Brocki, N.C. Chung, et al., Artificial intelligence: Deep learning in oncological radiomics and challenges of interpretability and data harmonization[J], Physica Medica 83 (2021) 108–121.
[21] E. Prifti, Y. Chevaleyre, B. Hanczar, et al., Interpretable and accurate prediction models for metagenomics data[J], GigaScience 9 (3) (2020) giaa010.
[22] A.M. DiGioia III, B. Jaramaz, B.D. Colgan, Computer-assisted orthopedic surgery: image-guided and robotic assistive technologies[J], Clinical Orthopaedics and Related Research® 354 (1998) 8–16.